ACS APPLIED MATERIALS & INTERFACES

Research Article

www.acsami.org

Microwave Annealing Effect for Highly Reliable Biosensor: Dual-Gate Ion-Sensitive Field-Effect Transistor Using Amorphous InGaZnO Thin-Film Transistor

In-Kyu Lee,[†] Kwan Hyi Lee,[‡] Seok Lee,[§] and Won-Ju Cho*[,†]

[†]Department of Electronic Materials Engineering, Kwangwoon University, 20 Gwangun-ro, Nowon-gu, Seoul 139-701, Republic of Korea

[‡]Biomedical Research Institute and [§]Sensor System Research Center, Korea Institute of Science and Technology (KIST), 5 Hwarang-ro 14-gil, Seongbuk-gu, Seoul 136-791, Republic of Korea

Supporting Information

ABSTRACT: We used a microwave annealing process to fabricate a highly reliable biosensor using amorphous-InGaZnO (a-IGZO) thin-film transistors (TFTs), which usually experience threshold voltage instability. Compared with furnace-annealed a-IGZO TFTs, the microwave-annealed devices showed superior threshold voltage stability and performance, including a high field-effect mobility of 9.51 $cm^2/V{\cdot}s$, a low threshold voltage of 0.99 V, a good subthreshold slope of 135 mV/dec, and an outstanding on/off current ratio of 1.18×10^8. In conclusion, by using the microwave-annealed a-IGZO TFT as the transducer in an extended-gate ion-sensitive field-effect transistor biosensor, we developed a high-performance biosensor with excellent sensing properties in terms of pH sensitivity, reliability, and chemical stability.

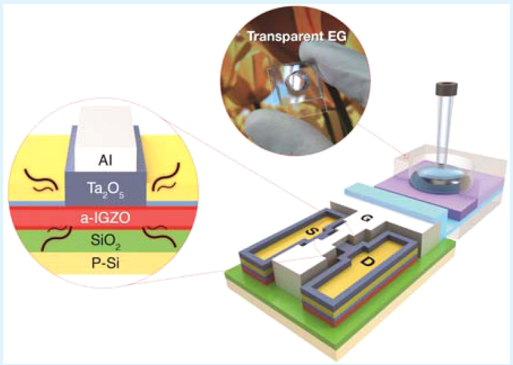

KEYWORDS: *microwave annealing, a-InGaZnO, dual gate ISFET, biosensor, reliability*

INTRODUCTION

Ion-sensitive field-effect transistors (ISFETs) are electrochemical sensors that convert a chemical signal into an electrical signal; Bergveld first proposed them in the 1970s.[1] The structure of ISFETs is based on metal-oxide semiconductor field-effect transistors (MOSFETs), in which the metal gate electrode is replaced by an electrolyte grounded with a reference electrode. The extended-gate field-effect transistors (EGFETs) are examples of ISFETs. They comprise an FET (transducer) and a sensing device (detector) that is separated from the FET to prevent it from being damaged by the chemical environment.[2,3] Although EGFETs have many advantages, including small size, low cost, rapid response, insensitivity to light, and compatibility with complementary metal-oxide semiconductor (CMOS) process, they have poor sensitivity, which limits the Nernstian pH response to 59 mV/pH at 25 °C, the maximum sensitivity achievable. For enhanced sensitivity that exceeds the Nernst limit, the dual-gate (DG) ISFET pH sensors, with silicon-on-insulator (SOI) substrates, were developed to replace the classic single-gate (SG) ISFETs on bulk-Si substrates.[4−7] The DG ISFETs can significantly amplify their sensitivity without additional amplification circuits by inducing capacitive coupling between the top and bottom gate oxides.[8,9] Especially, in biological sensing applications, the DG ISFETs have enormous potential because they can greatly enhance the small signals monitored during biological events such as nucleic acid hybridization, protein−protein interactions, enzyme−substrate reactions, and antigen−antibody binding.[10−14] However, SOI-based devices do have some issues, including the high cost of the SOI wafer, poor transparency, and difficulty in fine-tuning structures, such as the channel layer and buried oxide (BOX), which are involved in the capacitive coupling ratio.

Recently, devices based on transparent amorphous oxide semiconductors (AOSs) have received considerable attention as alternatives to conventional silicon-based devices. Among them, amorphous indium−gallium−zinc oxide (a-IGZO) thin-film transistors (TFTs) have been applied in various devices, such as phototransistors, nonvolatile memory devices, and biosensors,[15−17] because of their superior electrical and optical characteristics, including high field-effect mobility, outstanding transparency in the visible spectrum, and superior spatial uniformity. In particular, application of an a-IGZO TFT as a transparent biosensor could provide high reliability because it can detect optical and electrophysiological signals simultaneously that are caused by a chemical stimulus.[18,19] However, before using an a-IGZO TFT as a biosensor, the problem of threshold voltage instability of the TFT must be resolved.[20,21]

Received: October 3, 2014
Accepted: December 2, 2014
Published: December 2, 2014

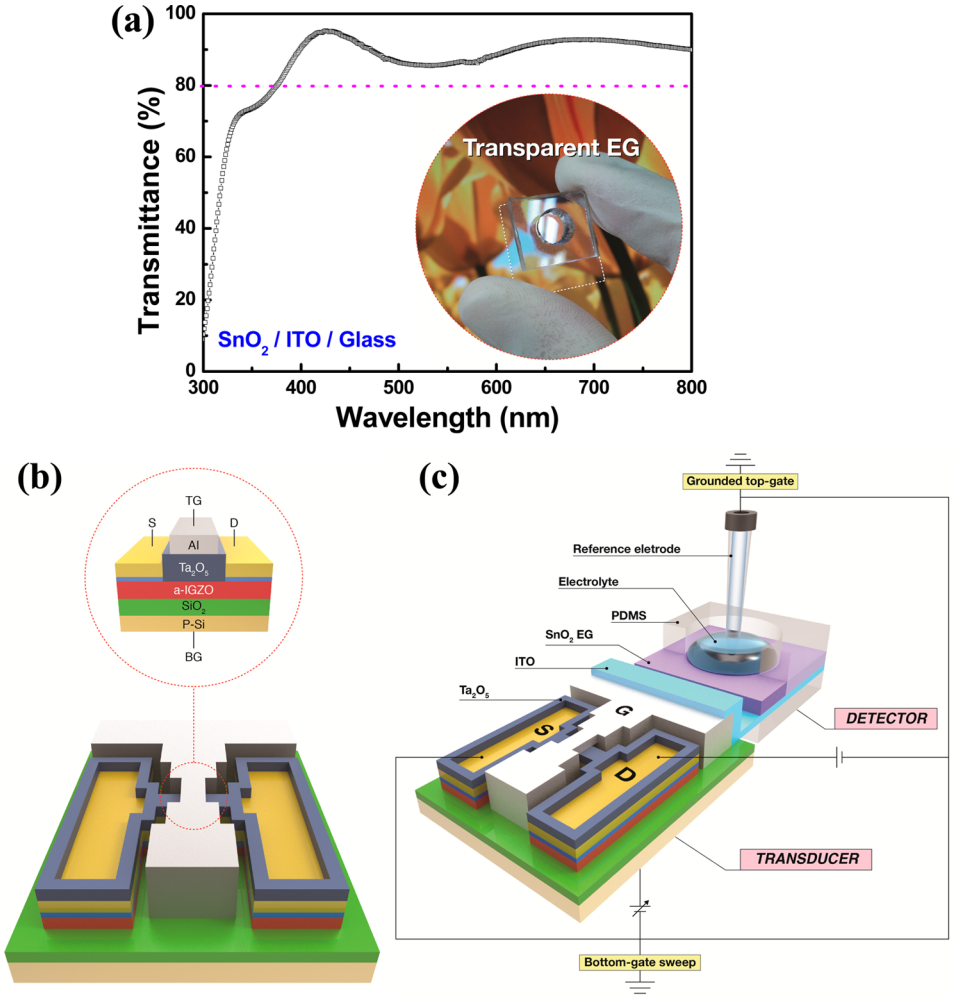

Figure 1. (a) Optical transmittance curve of the SnO_2/ITO films deposited on a glass substrate (inset shows fabricated transparent EG). Schematic illustrations of fabricated (b) a-IGZO TFTs and (c) EGFETs in DG operation mode.

For biosensor applications, this instability is one of the most critical considerations because it directly affects the reliability of the biosensors. To overcome this problem and achieve satisfactory performance and stability of the device, use of the high-temperature thermal annealing process at ∼600 °C is typically required.[22−24] However, the high-temperature thermal annealing process can also be limited for use in fabricating devices based on some transparent or flexible substrate such as glass, plastic, or paper.

We studied a microwave annealing process that can be used with various substrates because the low heating temperature used in the process would remedy this problem. The favorable characteristics of microwave annealing are that it is fast, has a low thermal budget, has a shorter manufacturing period, provides thermal uniformity, and suppresses diffusion of unexpected species.[25−27] With this process we were able to fabricate high-performance DG ISFET biosensors by improving the threshold voltage instability of a-IGZO TFTs.

EXPERIMENTAL SECTION

Fabrication of the EGFET Sensing Membrane. A 75 nm thick indium tin oxide (ITO) film, which serves as a metal that transmits the electrical potential variation on the surface of the sensing membrane to the gate electrode, was deposited on a clean glass substrate by radio frequency (RF) magnetron sputtering at room temperature. A 45 nm thick tin dioxide (SnO_2) film, a sensing membrane, was then formed on the ITO film on the glass substrate by RF magnetron sputtering, during which the RF power, chamber pressure, and Ar gas flow rate were 50 W, 3 mTorr, and 20 sccm, respectively. Finally, to inject the pH buffer solution, polydimethylsiloxane (PDMS), a reservoir, was attached onto the sensing membrane using silicone glue. The optical transmittance curve of the SnO_2/ITO films deposited on the glass substrate is shown in Figure 1a. The transmittance was greater than 80% in the visible light region.

Fabrication of a-IGZO TFTs as EGFET Transducer. Thermal oxide films that are 300 nm thick were grown on p-type bulk Si (100) wafers and had a resistivity of 10−20 Ω·cm. For the active layer, a 70 nm thick layer of a-IGZO ($In_2O_3/Ga_2O_3/ZnO$, target composition ratio = 1:1:1 mol %) was deposited by RF magnetron sputtering at room temperature. The initial vacuum level was less than 5×10^{-6} Torr, while the working pressure, RF power, and ambient Ar gas flow rate were set at 6 mTorr, 100 W, and 30 sccm, respectively. Presputtering was performed for 10 min before the active layer was deposited to remove any contamination on the target surface. Then, 10 nm thick titanium (Ti) and 60 nm thick gold (Au) layers were formed into the source and drain electrodes by the e-beam evaporation method. A 100 nm thick tantalum pentoxide (Ta_2O_5) layer was deposited by RF magnetron sputtering, with RF power set at 75 W, working pressure at 6 mTorr, and Ar flow rate of 20 sccm. The Ta_2O_5 film was used as a gate dielectric because of its high dielectric constant of ∼29.[28] A 150 nm thick aluminum (Al) gate electrode was made using the e-beam evaporation method and the image-reversal process of photolithography. The channel length and width of the fabricated a-IGZO TFTs were 10 and 20 μm, respectively. Finally, to remove any

intrinsic defects of a-IGZO or the gate dielectric and to improve the interface between the a-IGZO layer and the gate insulator, postdeposition annealing (PDA) was performed using a furnace annealing system and a microwave annealing system at a microwave frequency of 2.45 GHz. Furnace annealing was performed at 400 °C for 30 min in ambient N_2, and microwave annealing was performed at a microwave power level of 1000 W for 10 min. The maximum internal temperature of the microwave annealing system, as detected by thermal coupler, was ~87 °C. The fabricated a-IGZO TFTs and EGFETs (in DG operation mode) are illustrated in Figure 1b,c, respectively.

Measurements. An Agilent Hewlett-Packard 4156B semiconductor parameter analyzer was used to measure the electrical characteristics of the a-IGZO TFTs and the pH-sensing properties of the EGFETs. A commercial Ag/AgCl electrode was used as a reference electrode for the pH-sensing measurements. All measurements were performed in a dark box to avoid any interference from external factors such as light and electrical noise.

RESULTS AND DISCUSSION

Figure 2 shows the transfer characteristic (I_D–V_G) and the output characteristic (I_D–V_D) curves of the a-IGZO TFTs that

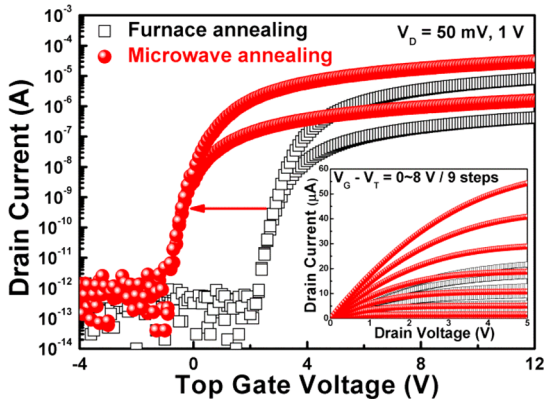

Figure 2. Transfer characteristics of a-IGZO TFTs annealed by microwave (red ●) and furnace (white □). (inset) The output characteristic curves of a-IGZO TFTs annealed by microwave (red ●) and furnace (white □).

were fabricated by furnace and microwave annealing. The devices were swept by top gate; the electrical parameters are summarized in Table 1. The microwave-annealed device

Table 1. Electrical Parameters of a-IGZO TFTs Annealed by a Microwave and a Furnace

annealing	mobility [cm^2/V·s]	V_t [V]	SS [V/dec]	on/off current ratio
microwave	9.51	0.99	0.13	1.18×10^8
furnace	4.51	4.85	0.15	3.38×10^7

(device A) exhibited better electrical properties than the furnace-annealed device (device B) with respect to device performance, despite a relatively low annealing temperature (87 °C) and a short processing time (10 min). This indicates that the microwave annealing process eliminates defects inside the device more effectively than the furnace annealing process.[25,26] Device A had a high field-effect mobility of 9.51 cm^2/V·s (drain voltage = 50 mV), a good subthreshold swing (SS) of 135 mV/dec, a low threshold voltage (V_{th}) of 0.99 V, and an excellent on/off current ratio of 1.18×10^8.

To investigate the defects that affect the threshold voltage instability of a-IGZO TFTs, the transfer curves were measured using a double-sweep mode. Figure 3a,b shows the hysteretic

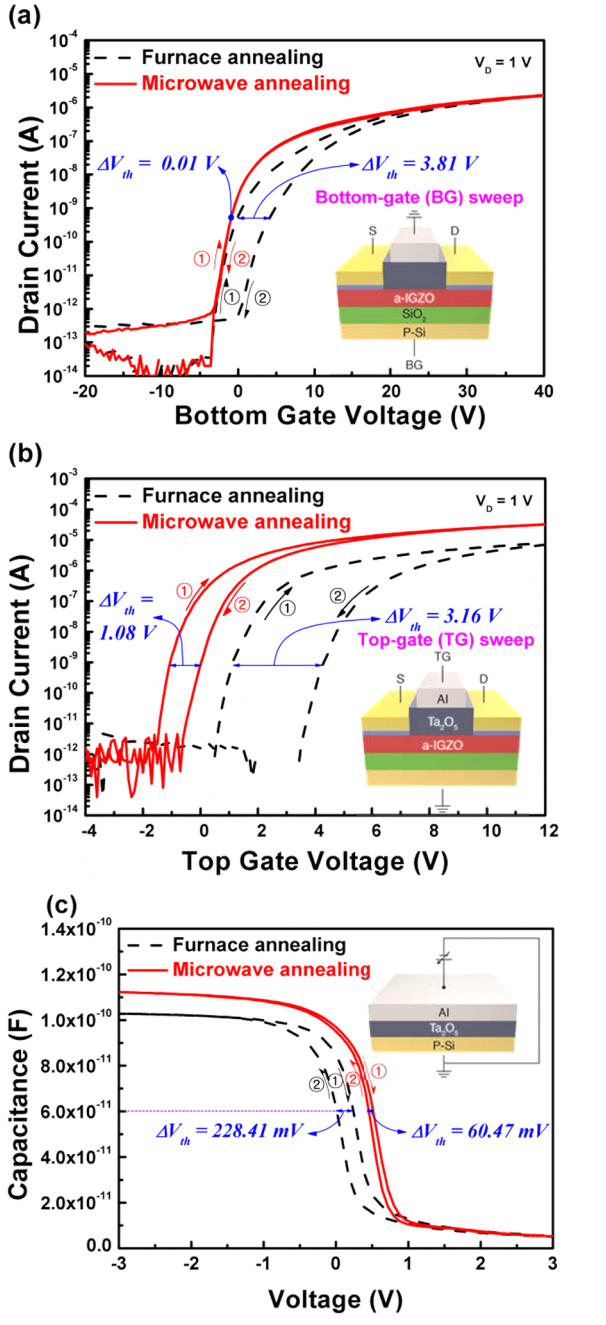

Figure 3. Hysteretic characteristics of a-IGZO TFTs annealed by microwave (red solid line) and furnace (black dashed line) in (a) BG and (b) TG sweep mode for the forward (①) and reverse (②) gate voltage sweep. (c) C–V curves of MIS capacitors with the structure of Al/Ta_2O_5/p-Si according to annealing method.

characteristics of the a-IGZO TFTs swept by bottom gate (BG) and top gate (TG), respectively. The electrical characteristics of a-IGZO TFTs with different annealing methods in BG and TG sweep mode, respectively, are given in Table 2.

The SS values of the devices were estimated using the following equation:

Table 2. Electrical Characteristics of a-IGZO TFTs According to Annealing Method in (a) BG and (b) TG Sweep Mode

sweep mode	annealing method	ΔV_{th} [V]	SS [V/dec], forward sweep	SS [V/dec], reverse sweep	ΔSS [V/dec]
(a) BG	microwave	0.01	0.26	0.27	0.01
	furnace	3.81	0.30	0.38	0.08
(b) TG	microwave	1.08	0.13	0.16	0.03
	furnace	3.16	0.15	0.24	0.09

$$SS = \frac{\partial V_{GS}}{\partial(\log I_{DS})} \quad (1)$$

where V_{GS} is the gate bias, which is the maximum slope in the transfer curve during forward and reverse sweeping. Thus, for the BG sweep mode (Figure 3a), device A exhibited a slight threshold voltage shift (ΔV_{th}) of 0.01 V and a small change in SS (ΔSS) of 0.01 V/dec, while device B had a ΔV_{th} of 3.81 V and a ΔSS of 0.08 V/dec The positive shift in V_{th} that accompanied the change in SS for device B during the double sweep is attributed to defects within the a-IGZO bulk and to negative charge carriers that were trapped at the a-IGZO/SiO_2 interface or injected into the SiO_2 bulk from the a-IGZO channel layer.[29] This means device B still had some defects after furnace annealing. On the other hand, the small hysteresis window and no change in SS for device A indicate that almost all defects in the a-IGZO bulk and at the a-IGZO/SiO_2 interface were eliminated.

Meanwhile, as seen in the inset of Figure 3b, the TG of a-IGZO TFTs was biased with grounded BG. Thus, device B had a ΔV_{th} of 3.16 V and a ΔSS of 0.09 V/dec, whereas device A had a relatively small ΔV_{th} of 1.08 V and a ΔSS of 0.03 V. (A similar trend in the results for device B in BG sweep mode can be seen.) An interesting phenomenon seen in the results is that in TG sweep mode, device A still had a hysteresis window and a small variation in SS, unlike in the BG sweep mode, although microwave annealing was performed. We conclude that these results derived from the simple charge trapping that occurred in the gate dielectric (Ta_2O_5) or at the a-IGZO/Ta_2O_5 interface because it is apparent from Figure 3a that the defects within the a-IGZO bulk were thoroughly eliminated by the microwave annealing. Furthermore, because there was no significant change in the SS value, the charge-trapping phenomenon in device A is thought to be associated mainly with the Ta_2O_5 bulk.

To further investigate the charge-trapping dynamics in the Ta_2O_5 bulk, we fabricated metal−insulator−semiconductor (MIS) capacitors (Figure 3c inset). The gate electrode and insulator of MIS capacitors were formed under the same processing conditions used for fabricating the TFTs; the fabricated capacitors were annealed using a furnace annealing system and a microwave annealing system. The size of the square electrode was 230 × 310 μm^2. Figure 3c shows the curve of C versus V measured at 1 MHz using an Agilent 4284A precision LCR meter. The hysteresis voltage (V_H) of the microwave-annealed capacitor was 60.47 mV, and that of the furnace-annealed capacitor was 228.41 mV. Even if the microwave-annealed device had relatively lower traps inside the Ta_2O_5 bulk compared with furnace-annealed devices, the former would still have a hysteresis window, which is consistent with the results shown in Figure 3b. Consequently, the remaining defects in device A after microwave annealing are caused by the Ta_2O_5 bulk. Thus, to use the fabricated a-IGZO TFTs in the transducer of EGFETs, the BG sweep mode is better than the TG sweep mode because of the enhanced reliability provided. To eliminate these charge-trapping defects in the Ta_2O_5 bulk and achieve stronger electrical characteristics, more studies are needed.

Figure 4 shows the bias-temperature-stress instability of the fabricated a-IGZO TFTs in BG sweep mode. In our study, we

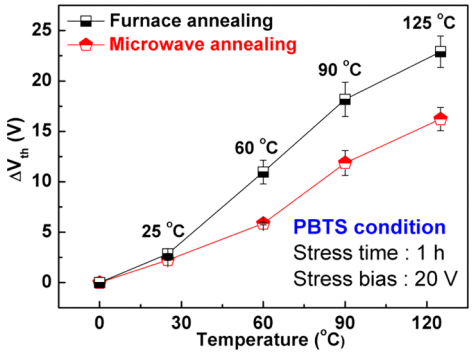

Figure 4. PBTS tests for the microwave-annealed device (half-filled □) and the furnace-annealed device (half filled ⬠) at various stress temperatures, including 25, 60, 90, and 125 °C.

performed only positive bias-temperature-stress (PBTS) measurements because the devices are influenced mainly by positive bias stress.[30,31] The devices were stressed under the following conditions: V_{GS} = +20 V, V_{DS} = 0 V, stress time = 1 h, and stress temperatures of 25, 60, 90, and 125 °C. Compared to that in device A, the V_{th} shift ($\Delta V_{th} = V_{sth} - V_{ith}$, where V_{sth} and V_{ith} are the threshold voltages after 1 h of stress and at the initial state, respectively) in device B increased largely with stress temperature, indicating that the threshold voltage instability of a-IGZO TFTs can improve with the use of microwave annealing.

Figure 5 shows the I_D−V_G curves of EGFETs with device A (Figure 5a) and device B (Figure 5b). The EGFETs were operated in SG (data not shown) and DG modes, respectively. Unlike the conventional SG operation (where the top reference electrode was biased), the DG operation, as shown in Figure 1c, was conducted by biasing the BG of a-IGZO TFTs with a grounded top reference electrode (see the Supporting Information, Figure S1). Thus, in both SG and DG modes, the reference voltage (V_R) of EGFETs shifted in a regular manner by varying the pH from 3 to 10. Here, V_R was defined as the gate voltage, where the drain current (reference current) was 3 or 6 μA in SG mode and 10 μA in DG mode under a drain voltage of 1 V. The sensing properties of SG and DG EGFETs with devices A and B are summarized in Table 3 for comparison.

In the SG mode, the sensitivity of EGFETs with device B was 101.27 mV/pH (data not shown), which is an abnormal value beyond the limit of the Nernstian pH response, which has a theoretical maximum value of 59 mV/pH (see the Supporting Information, Figure S2a). This abnormal sensitivity value occurred because the V_{th} instability of device B affected the ΔV_R of the EGFETs. On the other hand, the EGFETs with device A had a pH sensitivity of 57.73 mV/pH, which was very high but within the normal pH response range (see the Supporting Information, Figure S2b). These results suggest that device A is an adequate transducer for EGFETs in terms of

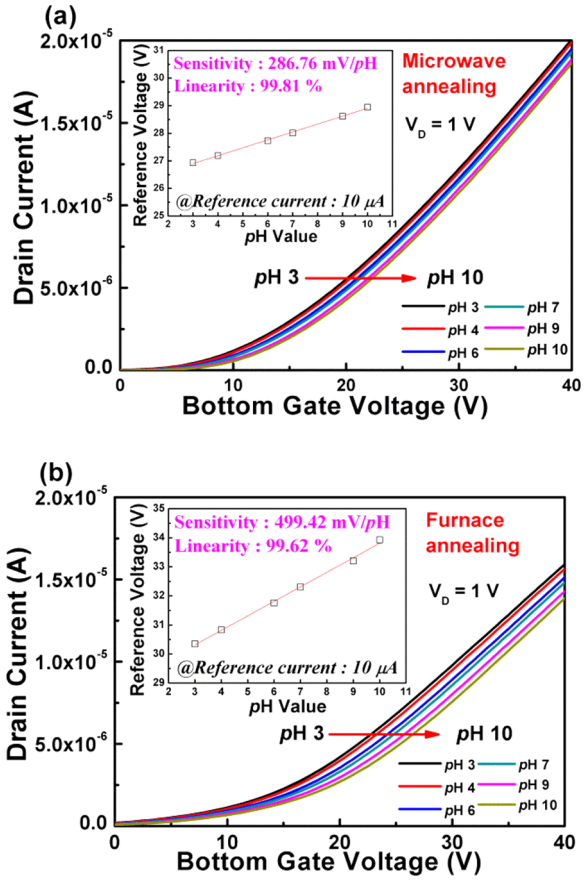

Figure 5. I_D−V_G curves of EGFETs with (a) device A and (b) device B for different pH buffer solutions. The drain bias is set at 1 V. The response voltage (V_R) for each pH buffer solution, shown in the inset, was defined as the corresponding gate voltage to the drain current (reference current: I_R) of 10 μA.

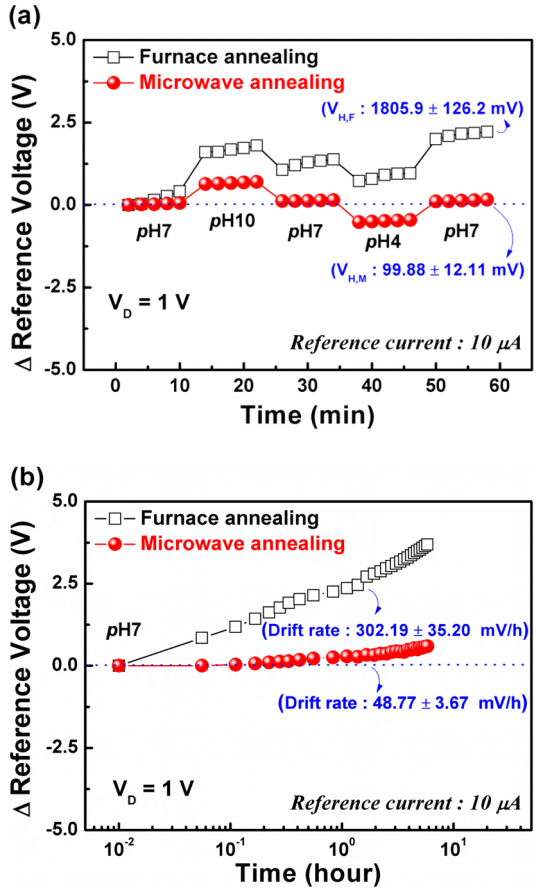

Figure 6. (a) Hysteresis phenomenon of EGFETs with device A (red ●) and device B (white □) for three buffer solutions. The EGFETs were subjected to the pH loop of 7−10−7−4−7 for 60 min. (b) Drift characteristics of EGFETs using device A and device B in a pH 7 buffer solution for 6 h.

reliability. Meanwhile, in the DG operation mode, the pH sensitivity was ∼5 times greater than that in the SG mode. The sensitivity of DG EGFETs with device A was 286.76 mV/pH (Figure 5a) and with device B 499.42 mV/pH (Figure 5b). We presented the details on the amplification of sensitivity by capacitive coupling between the top and bottom gate oxides in DG EGFETs in our previous work.[6,7,9,32] Consequently, these results for DG EGFETs are consistent with those for SG EGFETs.

Figure 6 shows the hysteresis phenomenon (Figure 6a) and the drift characteristics (Figure 6b) of the EGFETs with devices A and B. The hysteresis phenomenon is an indicator to evaluate the reliability of the devices by repetitive variation of the pH for a short time, and it is defined as the difference between the reference voltages in the first and last pH 7 solutions during the pH loop of 7−10−7−4−7.[33] We investigated the transition of the reference voltages by measuring them five times per pH value at 2 min intervals. The EGFETs with device A had a much lower hysteresis voltage with respect to sensitivity ($V_{H,SG}$ = 25.28 mV and $V_{H,DG}$ = 99.88 mV) than EGFETs with device B ($V_{H,SG}$ = 763.78 mV and $V_{H,DG}$ = 1805.90 mV). To compare the degree of hysteresis phenomenon of each device in SG or DG operation, the percentage of variation of V_H for the respective sensitivity is taken into consideration. As a result, the DG EGFETs with device A showed the best reliability. Meanwhile, the drift effect is used to evaluate the long-term chemical stability of sensors and is defined as the rate of variation in the maximum and minimum reference voltages for only one type of pH buffer solution.[34] In this work, we observed the tendency of the reference voltages to change in pH 7 buffer solution over 6 h. As a result, the DG EGFETs with device A had the lowest drift rate at a sensitivity of 17.04%, which means that these devices have better long-term chemical stability than any other device. In conclusion, with respect to pH sensitivity, reliability, and chemical stability, the DG EGFETs with device A had superior sensing properties.

Table 3. Sensing Properties of (a) SG and (b) DG EGFETs Using Devices A and B

operation mode	transducer	sensitivity (nA/pH)	linearity (%)	V_H (mV)	drift rate (mV/h)	V_H for sensitivity (%)	drift rate for sensitivity (%)
(a) SG	device A	57.77	99.38	25.28	25.80	43.76	44.66
	device B	101.27	99.27	763.78	138.66	754.20	136.92
(b) DG	device A	286.76	99.81	99.88	48.77	34.83	17.01
	device B	499.42	99.42	1805.9	302.19	361.60	60.51

dx.doi.org/10.1021/am506805a | ACS Appl. Mater. Interfaces 2014, 6, 22680−22686

CONCLUSION

In this work, we investigated how microwave annealing improved the threshold voltage instability of a-IGZO TFTs. The a-IGZO TFTs fabricated by microwave annealing exhibited enhanced device performance, including mobility of 9.51 $cm^2/V{\cdot}s$ and an on/off current ratio of 1.18×10^8. In contrast with the furnace-annealed devices, the threshold voltage instability of microwave-annealed a-IGZO TFTs was greatly improved because of the elimination of defects inside the a-IGZO TFT by microwave annealing. On the basis of our results, we used the microwave-annealed a-IGZO TFTs as the transducer of EGFET biosensors. The DG EGFETs with microwave-annealed a-IGZO TFTs had excellent sensing properties in terms of pH sensitivity, reliability, and chemical stability. Kim et al. discussed recent advances and developments in the bioanalytical technology of ISFET-based biosensors.[10] The pH-based transistor biosensors are well-represented in their literature. For example, enzyme-based ISFET has the same principle as that of pH-sensitive ISFETs because the concentration of hydrogen ions changes in proportion to the level of substrate curing an enzymatic reaction. Also, the pH-based ISFETs can be used as an immunosensor detecting the charge variation induced by the antigen−antibody interaction after attaching the antibodies on the surface. This means that a-IGZO TFT-based pH sensors fabricated in this work can be used to detect various biological events. Therefore, we believe that the DG EGFETs with microwave-annealed a-IGZO TFT provide a novel path to biosensor applications with high reliability and stability.

ASSOCIATED CONTENT

Supporting Information

Schematic representation of EGFETs with (a) SG and (b) DG operation mode, I_D-V_G curves of SG-EGFETs using furnace-annealed and microwave-annealed a-IGZO TFTs for different pH buffer solutions, hysteresis phenomenon and drift characteristics of SG-EGFETs with furnace-annealed and microwave-annealed a-IGZO TFTs. This material is available free of charge via the Internet at http://pubs.acs.org.

AUTHOR INFORMATION

Corresponding Author

*E-mail address: chowj@kw.ac.kr.

Notes

The authors declare no competing financial interest.

ACKNOWLEDGMENTS

This work was supported by the KIST Open Research Program (Project No. 2E25191). The authors deeply appreciate Mr. S.-C. Mun's cooperation.

REFERENCES

(1) Bergveld, P. Development of an Ion-Sensitive Solid-State Device for Neurophysiological Measurements. *IEEE Trans. Biomed. Eng.* **1970**, *1*, 70−71.

(2) Chi, L. L.; Chou, J. C.; Chung, W. Y.; Sun, T. P.; Hsiung, S. K. Study on Extended Gate Field Effect Transistor with Tin Oxide Sensing Membrane. *Mater. Chem. Phys.* **2000**, *63*, 19−23.

(3) Yin, L. T.; Chou, J. C.; Chung, W. Y.; Sun, T. P.; Hsiung, S. K. Separate Structure Extended Gate H^+-Ion Sensitive Field Effect Transistor on a Glass Substrate. *Sens. Actuators, B* **2000**, *71*, 106−111.

(4) Knopfmacher, O.; Tarasov, A.; Fu, W.; Wipf, M.; Niesen, B.; Calame, M.; Schonenberger, C. Nernst Limit in Dual-Gated Si-Nanowire FET Sensors. *Nano Lett.* **2010**, *10*, 2268−2274.

(5) Spijkman, M.; Smits, E. C. P.; Cillessen, J. F. M.; Biscarini, F.; Blom, P. W. M.; de Leeuw, D. M. Beyond the Nernst-Limit with Dual-Gate ZnO Ion-Sensitive Field-Effect Transistors. *Appl. Phys. Lett.* **2011**, *98*, 043502−043502.

(6) Jang, H. J.; Bae, T. E.; Cho, W. J. Improved Sensing Performance of Polycrystalline-Silicon Based Dual-Gate Ion-Sensitive Field-Effect Transistors Using High-k Stacking Engineered Sensing Membrane. *Appl. Phys. Lett.* **2012**, *100*, 253703.

(7) Park, J. K.; Jang, H. J.; Park, J. T.; Cho, W. J. SOI Dual-Gate ISFET with Variable Oxide Capacitance and Channel Thickness. *Solid-State Electron.* **2014**, *97*, 2−7.

(8) Spijkman, M. J.; Myny, K.; Smits, E. C.; Heremans, P.; Blom, P. W.; de Leeuw, D. M. Dual-Gate Thin-Film Transistors, Integrated Circuits and Sensors. *Adv. Mater.* **2011**, *23*, 3231−3242.

(9) Jang, H. J.; Cho, W. J. Performance Enhancement of Capacitive-Coupling Dual-gate Ion-Sensitive Field-Effect Transistor in Ultra-Thin-Body. *Sci. Rep.* **2014**, *4*, 5284.

(10) Lee, C. S.; Kim, S. K.; Kim, M. Ion-Sensitive Field-Effect Transistor for Biological Sensing. *Sensors* **2009**, *9*, 7111−7131.

(11) Goncalves, D.; Prazeres, D. M. F.; Chu, V.; Conde, J. P. Detection of DNA and Proteins Using Amorphous Silicon Ion-Sensitive Thin-Film Field Effect Transistors. *Biosens. Bioelectron.* **2008**, *24*, 545−551.

(12) Mao, S.; Lu, G.; Yu, K.; Bo, Z.; Chen, J. Specific Protein Detection Using Thermally Reduced Graphene Oxide Sheet Decorated with Gold Nanoparticle-Antibody Conjugates. *Adv. Mater.* **2010**, *22*, 3521−3526.

(13) Liu, X.; Lin, P.; Yan, X.; Kang, Z.; Zhao, Y.; Lei, Y.; Li, C.; Du, H.; Zhang, Y. Enzyme-Coated Single ZnO Nanowire FET Biosensor for Detection of Uric Acid. *Sens. Actuators, B* **2013**, *176*, 22−27.

(14) Li, B. R.; Hsieh, Y. J.; Chen, Y. X.; Chung, Y. T.; Pan, C. Y.; Chen, Y. T. An Ultrasensitive Nanowire-Transistor Biosensor for Detecting Dopamine Release from Living PC12 Cells under Hypoxic Stimulation. *J. Am. Chem. Soc.* **2013**, *135*, 16034−16037.

(15) Chang, T. H.; Chiu, C. J.; Weng, W. Y.; Chang, S. J.; Tsai, T. Y.; Huang, Z. D. High Responsivity of Amorphous Indium Gallium Zinc Oxide Phototransistor with Ta_2O_5 Gate Dielectric. *Appl. Phys. Lett.* **2012**, *101*, 261112.

(16) Yin, H.; Kim, S.; Lim, H.; Min, Y.; Kim, C. J.; Song, I.; Park, J.; Kim, S. W.; Tikhonovsky, A.; Hyun, J.; Park, Y. Program/Erase Characteristics of Amorphous Gallium Indium Zinc Oxide Nonvolatile Memory. *IEEE Trans. Electron Devices* **2008**, *55*, 2071−2077.

(17) Kim, S. J.; Jung, J.; Lee, K. W.; Yoon, D. H.; Jung, T. S.; Dugasani, S. R.; Park, S. H.; Kim, H. J. Low-Cost Label-Free Electrical Detection of Artificial DNA Nanostructures Using Solution-Processed Oxide Thin-Film Transistors. *ACS Appl. Mater. Interfaces* **2013**, *5*, 10715−10720.

(18) Kim, S. J.; Jung, J.; Yoon, D. H.; Kim, H. J. The Effect of Various Solvents on the Back Channel of Solution-Processed In−Ga−Zn−O Thin-Film Transistors Intended for Biosensor Applications. *J. Phys. D: Appl. Phys.* **2013**, *46*, 035102.

(19) Tonomura, W.; Okamura, H.; Konishi, S. Transparent Biosensor with Micro Channel Array for Optical and Electrophysiological Detection of Luciferin−Luciferase Reaction. *IEEJ. Trans. Electr. Electron. Eng.* **2007**, *2*, 372−377.

(20) Bak, J. Y.; Yang, S.; Ryu, M. K.; Ko Park, S. H.; Hwang, C. S.; Yoon, S. M. Effect of the Electrode Materials on the Drain-Bias Stress Instabilities of In−Ga−Zn−O Thin-Film Transistors. *ACS Appl. Mater. Interfaces* **2012**, *4*, 5369−5374.

(21) Kwon, J. M.; Jung, J.; Rim, Y. S.; Kim, D. L.; Kim, H. J. Improvement in Negative Bias Stress Stability of Solution-Processed Amorphous In−Ga−Zn−O Thin-Film Transistors Using Hydrogen Peroxide. *ACS Appl. Mater. Interfaces* **2014**, *6*, 3371−3377.

(22) Chen, W. T.; Lo, S. Y.; Kao, S. C.; Zan, H. W.; Tsai, C. C.; Lin, J. H.; Fang, C. H.; Lee, C. C. Oxygen-Dependent Instability and

Annealing/Passivation Effects in Amorphous In−Ga−Zn−O Thin-Film Transistors. *IEEE Electron Device Lett.* **2011**, *32*, 1552−1554.
(23) Nomura, K.; Kamiya, T.; Kikuchi, Y.; Hirano, M.; Hosono, H. Comprehensive Studies on the Stabilities of a-In-Ga-Zn-O Based Thin Film Transistor by Constant Current Stress. *Thin Solid Films* **2010**, *518*, 3012−3016.
(24) Fuh, C. S.; Sze, S. M.; Liu, P. T.; Teng, L. F.; Chou, Y. T. Role of Environmental and Annealing Conditions on the Passivation-Free In-Ga−Zn−O TFT. *Thin Solid Films* **2011**, *520*, 1489−1494.
(25) Teng, L. F.; Liu, P. T.; Lo, Y. J.; Lee, Y. J. Effects of Microwave Annealing on Electrical Enhancement of Amorphous Oxide Semiconductor Thin Film Transistor. *Appl. Phys. Lett.* **2012**, *101*, 132901.
(26) Fuh, C. S.; Liu, P. T.; Teng, L. F.; Huang, S. W.; Lee, Y. J.; Shieh, H. P.; Sze, S. M. Effects of Microwave Annealing on Nitrogenated Amorphous In-Ga-Zn-O Thin-Film Transistor for Low Thermal Budget Process Application. *IEEE Electron Device Lett.* **2013**, *34*, 1157−1159.
(27) Cheng, H. C.; Tsay, C. Y. Flexible a-IZO Thin Film Transistors Fabricated by Solution Processes. *J. Alloys Compd.* **2010**, *507*, L1−L3.
(28) Chiu, C. J.; Chang, S. P.; Chang, S. J. High-Performance a-IGZO Thin-Film Transistor Using Ta_2O_5 Gate Dielectric. *IEEE Electron Device Lett.* **2010**, *31*, 1245−1247.
(29) Jeong, J. K.; Yang, H. W.; Jeong, J. H.; Mo, Y. G.; Kim, H. D. Origin of Threshold Voltage Instability in Indium-Gallium-Zinc Oxide Thin Film Transistors. *Appl. Phys. Lett.* **2008**, *93*, 123508.
(30) Ryu, M. K.; Ko Park, S. H.; Hwang, C. S.; Yoon, S. M. Comparative Studies on Electrical Bias Temperature Instabilities of In−Ga−Zn−O Thin Film Transistors with Different Device Configurations. *Solid-State Electron.* **2013**, *89*, 171−176.
(31) Lee, I. K.; Lee, S. W.; Gu, J. G.; Kim, K. S.; Cho, W. J. Comparative Study of Device Performance and Reliability in Amorphous InGaZnO Thin-Film Transistors with Various High-k Gate Dielectrics. *Jpn. J. Appl. Phys.* **2013**, *52*, 06GE05.
(32) Bae, T. E.; Cho, W. J. Enhanced Sensing Properties of Fully Depleted Silicon-on-Insulator-Based Extended-Gate Field-Effect Transistor with Dual-Gate Operation. *Appl. Phys. Express* **2013**, *6*, 127001.
(33) Bousse, L.; Mostarshed, S.; van der Schoot, B.; De Rooij, N. F. Comparison of the Hysteresis of Ta_2O_5 and Si_3N_4 pH-Sensing Insulators. *Sens. Actuators, B* **1994**, *17*, 157−164.
(34) Chiang, J. L.; Chou, J. C.; Chen, Y. C.; Liau, G. S.; Cheng, C. C. Drift and Hysteresis Effects on AlN/SiO_2 Gate pH Ion-Sensitive Field-Effect Transistor. *Jpn. J. Appl. Phys.* **2003**, *42*, 4973.

NOTE ADDED AFTER ASAP PUBLICATION

This paper was published on the Web on December 11, 2014, with errors in Figure 6b. The corrected version was reposted on December 24, 2014.